Determination of the exchange constant of $Tb_{0.3}Dy_{0.7}Fe_2$ by broadband ferromagnetic resonance spectroscopy

D. B. Gopman,[1,*] J. W. Lau,[1] K. P. Mohanchandra,[2] K. Wetzlar,[2] and G. P. Carman[2]
[1]*Materials Science and Engineering Division, NIST, Gaithersburg, Maryland 20899, USA*
[2]*Department of Mechanical and Aerospace Engineering, University of California, Los Angeles, California 90095, USA*
(Received 18 December 2015; revised manuscript received 2 February 2016; published 23 February 2016)

We present measurements of the exchange stiffness D and the exchange constant A of a sputtered 80 nm $Tb_{0.3}Dy_{0.7}Fe_2$ film. Using a broadband ferromagnetic resonance setup in a wide frequency range from 10 to 50 GHz, multiple perpendicular standing spin-wave resonances were observed with the external static magnetic field applied in-plane. The field corresponding to the strongest resonance peak at each frequency is used to determine the effective magnetization, the g factor, and the Gilbert damping. Furthermore, the dependence of spin-wave mode on field position is observed for several frequencies. The analysis of spin-wave resonance spectra at multiple frequencies allows precise determination of the exchange stiffness $D = (2.79 \pm 0.02) \times 10^{-17}$ T m^2 for an 80 nm thick film. From this value, we calculated the exchange constant $A = (9.1 \pm 0.1)$ pJ m^{-1}.

DOI: 10.1103/PhysRevB.93.064425

Strain-mediated, multiferroic composites combining nanoscale ferroelectric and ferromagnetic materials show great promise due to the vast range of functionalities that can be simultaneously harnessed. Novel technologies based on these multifunctional materials have recently been envisioned in memory [1–3], sensors [4–6], transducers [7–9], and spintronics [4,10–12]. Key to each of these technologies is the efficient transduction of energy between ferroic order parameters, most notably the generation or modulation of nanoscale magnetism by electrically actuated mechanical effects. This will require the controlled growth and characterization of magnetic phases with known material properties.

The most promising aspect of such multiferroic composites is the nonlinear magnetic response seen in ferromagnetic micro- and nanostructures, especially as it pertains to the dynamic behavior of highly magnetoelastic rare-earth alloys and compounds. In order to fully understand the physics of these highly coupled magnetic systems, fully dynamic models were developed using a Landau-Lifschitz-Gilbert (LLG) based finite element framework [13]. This technique allowed for the simulation of domain reversal processes in continuous and patterned thin films [14,15], the effects of mechanical strain on magnetic equilibrium and coercivity [16–18], and the incorporation of fully coupled micromechanical phenomena [19–22]. While these models do an excellent job of predicting complicated nonlinear response at the nanoscale in magnetoelastic materials, the knowledge of certain vital material properties used in the models remain absent from the literature.

Accurate values for a given material or compound's static and dynamic magnetic properties are a key requirement for predictive micromagnetic models. This includes static properties such as saturation magnetization, anisotropy field(s), and quasistatic magnetoelastic coupling coefficients, along with dynamic properties including Gilbert damping, the spectroscopic g factor, and the exchange stiffness. The last parameter is particularly important, as it determines the most energetically favorable magnetic configurations in nanoscale magnetic objects, for example in nanorings [23,24] and nanopillars [25]. With regards to the magnetic transition metals (Ni, Fe, and Co) and their alloys, these properties have been studied extensively; however, their rare-earth counterparts have only just begun to be critically examined, especially as it pertains to their dynamic properties.

The rare-earth compound $Tb_{0.3}Dy_{0.7}Fe_2$ (Terfenol-D) produces the largest magnetoelastic response of any soft ferromagnetic material presently available. While the macroscopic magnetic and mechanical properties of Terfenol-D have generated substantial attention, few papers evaluate the response of thin film or nanostructured Terfenol-D elements. Specifically, dynamic properties such as the exchange length have not been rigorously evaluated for use in analysis necessary to understand and design Terfenol-D at the nanoscale. In previous modeling efforts [17,26–29], estimations of the dynamic magnetic properties of Terfenol-D films have been accomplished using properties between nickel and iron, or measured in bulk twinned single crystals [30], but experiments have found poor correlations to models utilizing these estimates. Thin films of Terfenol-D are typically produced pseudo-amorphous and polycrystalline by a variety of techniques [31–34]. A parametric study of sputtering deposition parameters and their resultant static magnetization characteristics was recently performed by Mohanchandra *et al* [35]. However, as of this letter, the dynamic properties of thin film Terfenol-D needed for accurate understanding and predictive modeling remain unknown.

In this paper, we evaluate the dynamic properties of Terfenol-D. Using dc magnetron sputtering and a post-growth annealing process described elsewhere, we grew the following trilayer on thermally oxidized Si(100): Ta (10 nm)/Terfenol-D (80 nm)/Ta (10 nm) [35]. The dynamical properties were studied using broadband ferromagnetic resonance spectroscopy, schematically depicted in Fig. 1. At fixed microwave excitation frequencies between 10 and 50 GHz, we sweep the applied in-plane magnetic field and record the position of Lorentzian-shaped absorption modes. We observed a high-field, large amplitude mode and lower-field, smaller amplitude modes. The frequency dependence of the high-field, large amplitude mode is related to the various dynamic properties of Terfenol-D

*daniel.gopman@nist.gov

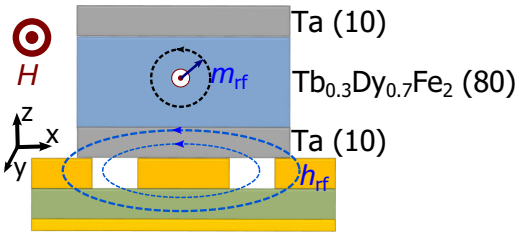

FIG. 1. Schematic of the experimental setup for broadband ferromagnetic resonance. The Ta/Terfenol-D/Ta trilayer (thicknesses indicated in nm) is placed film side down onto a grounded coplanar waveguide with a fixed frequency microwave magnetic field h_{rf} along the x direction. Additionally, there is an applied in-plane field H along the y axis. By varying H, the dynamic magnetization m_{rf} is brought into resonance with h_{rf}.

(magnetic anisotropy, g factor, and Gilbert damping). The additional modes originate in perpendicular standing spin-wave (PSSW) modes and their separation from the high-field mode is related to the exchange stiffness. We evaluate the mode dependence of the first few PSSW modes at a series of microwave frequencies to determine the exchange stiffness constant, D [36–39]. From this value, we calculate the exchange constant A.

The Kittel equation for ferromagnetic resonance governs the relationship between microwave excitation frequency and resonant applied magnetic field for fields applied in the plane [40]:

$$\left(\frac{2\pi f}{\gamma}\right)^2 = \mu_0^2(H_{res} + H_{ip})(H_{res} + H_{ip} + H_K + M_s), \quad (1)$$

where $\gamma = g\mu_B/\hbar$ is the gyromagnetic ratio, g is the g factor, μ_B is the Bohr magneton, $\hbar$ is the reduced Planck constant, μ_0 is the vacuum permeability, H_{ip} reflects the in-plane magnetic anisotropy, H_K reflects the uniaxial magnetic anisotropy, and M_S is the saturation magnetization. Figure 2(a) shows two exemplary absorption spectra at 35 and 40 GHz used to determine the resonant field and linewidth at each frequency. An excitation field ($f = 277$ Hz, $B_{pk} = 1$ mT) collinear to the dc magnetic field is generated for lock-in detection of the differential absorption versus applied magnetic field. The $k = 0$ ferromagnetic resonance mode, as well as additional resonance modes for each microwave frequency, is obtained by fitting the absorption data to a sum of Lorentzian curves [38]. In Fig. 2(b), we plot the frequency dependence of the ferromagnetic resonance field from 10 to 50 GHz, using Eq. (1) to obtain a best-fit curve plotted on top of the data points. Using an empirically determined M_S of (670 ± 10) kA/m from superconducting quantum interference device magnetometry, we estimate $\mu_0 H_K = 1.7 \pm 0.3$ T, $\mu_0 H_{ip} = 1.0 \pm 0.3$ T, and $g = 2.3 \pm 0.1$. Error bars reflect one standard deviation of the regression fit plus the uncertainty of the extracted resonance field and linewidth at each frequency. We observe an in-plane anisotropy energy (400 ± 100 kJ/m^3) consistent with previous reports on Terfenol-D [30,34,41]. Furthermore, we have estimated the Gilbert damping by fitting the linear frequency

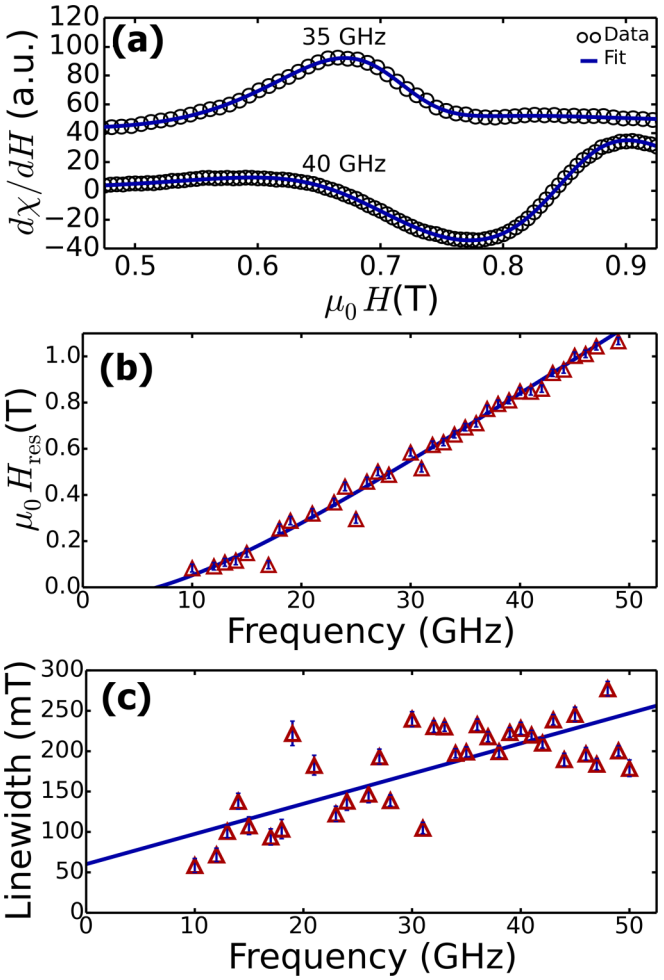

FIG. 2. (a) Ferromagnetic resonance spectra at $f = 35$ and 40 GHz (open circles). Best-fit lines (blue lines) are the sum of multiple derivative Lorentzian functions. (b) The microwave frequency versus $k = 0$ ferromagnetic resonance field (red triangles) and (c) $k = 0$ mode linewidth versus frequency extracted from the multiple spin-wave mode spectra. Blue lines are the best-fit to Eqs. (1) and (2) respectively.

dependence of measured resonance linewidth ΔH:

$$\Delta H = \frac{4\pi\alpha f}{\gamma\mu_0} + \Delta H_0. \quad (2)$$

Figure 2(c) shows the data and the best-fit line. From these results, a Gilbert damping factor of $\alpha = 0.06 \pm 0.02$ and an inhomogeneous broadening of $\Delta H_0 = 0.06 \pm 0.01$ T is determined. It should be mentioned that the estimated Gilbert damping here is lower by a factor of 1/3 from what has been assumed in recent models using Terfenol-D [28,29].

In addition to the ferromagnetic resonance mode whose frequency dependence was shown in Fig. 2(b), we also observed satellite peaks in the absorption scans at several microwave excitation frequencies. Figure 3 shows an exemplary absorption scan at $f = 40$ GHz with arrows representing resonance modes. The primary absorption peak at $\mu_0 H_{res} = 0.863$ T is accompanied by multiple modes appearing at applied magnetic fields both above and below the uniform Kittel mode. The peaks located at lower applied fields

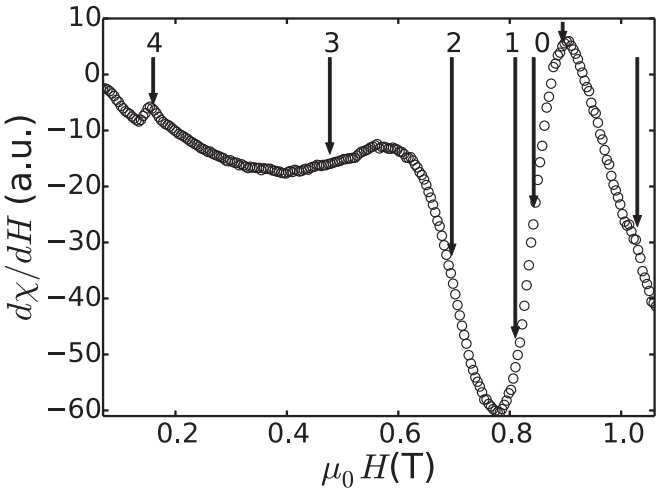

FIG. 3. Spin-wave resonances versus applied in-plane field at $f = 40$ GHz. Arrows indicate resonance field positions labeled by their mode number n.

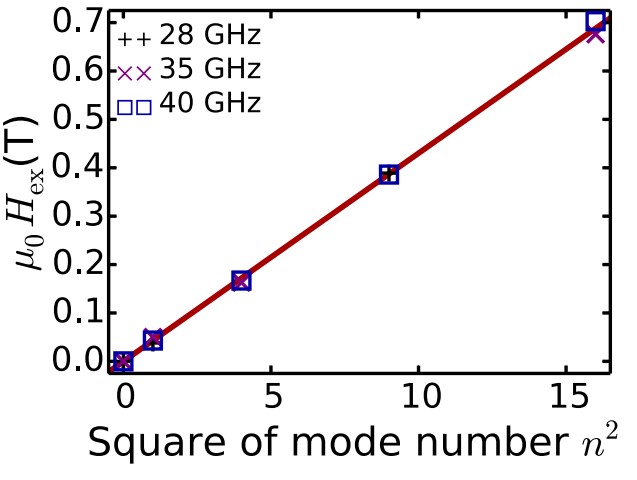

FIG. 4. Exchange field versus square of the mode number for $f = 28$ GHz (black plus markers), 35 GHz (purple crosses), and 40 GHz (blue squares). The red line is the best fit to Eq. (4).

are associated with perpendicular standing spin-wave modes (mode number n is indicated on Fig. 3) extending through the 80 nm Terfenol-D thickness and corresponding to real-valued wave vector $k = n\pi/d$, where d is the film thickness. The peaks appearing at higher applied fields may originate from a surface spin-wave mode or from predicted interferences between spin waves and acoustic waves propagating within the highly magnetoelastic Terfenol-D film [37,42]. The position of the thickness spin-wave modes and their relationship to the ferromagnetic resonance can be evaluated by the expression

$$H_{\text{res}} + H_{\text{ex}}(k) = H_{\text{ex}}^0, \tag{3}$$

where H_{ex}^0 is the $k = 0$ ferromagnetic resonance field and $H_{\text{ex}}(k)$ is the exchange field of the kth spin-wave mode. This exchange field splitting is described by the expression

$$H_{\text{ex}}(k) = Dk^2, \tag{4}$$

where D is the exchange stiffness.

A subtraction method is used for evaluating the exchange stiffness from the resonant field separation of higher-order spin-wave modes from the $k = 0$ ferromagnetic resonance mode [39,43]. Here the exchange field $H_{\text{ex}}(k)$ is defined in terms of the shift from the $k = 0$ ferromagnetic resonance field, with assumptions about M_{eff} and g removed from the analysis. Moreover, the exchange field shift should be the same for all excitation frequencies, although the amplitude of the distinct modes and their linewidths may vary [38]. This permits us to use the exchange field shift data at multiple frequencies to determine the exchange stiffness. Figure 4 presents the exchange field shifts versus the mode number squared for spectra obtained at $f = 28$, 35, and 40 GHz. The best linear fit to the data is plotted as a solid line, from which the slope of the line permits estimation of the exchange stiffness $D = (2.79 \pm 0.02) \times 10^{-17}$ T m^2.

In order to determine the exchange constant $A = DM_S/2$ of this Terfenol-D film, the saturation magnetization M_S must also be known. Superconducting quantum interference device magnetometry was used to determine $M_S = (670 \pm 10)$ kA/m, which is consistent with values achieved in sputtered and in evaporated Terfenol-D films [34,44]. Finally, we estimate the exchange constant $A = (9.4 \pm 0.1)$ pJ m^{-1}.

In conclusion, we have determined the exchange constant of an 80 nm thick Terfenol-D film using broadband ferromagnetic resonance spectroscopy. The dynamic measurements reported in this letter also enabled determination of other key magnetic parameters (magnetic anisotropy, g factor, Gilbert damping) relevant to fast operation of new devices based on Terfenol-D. These findings are an important step for gaining a better picture of spin dynamics and relaxation in Terfenol-D films and especially, setting up accurate predictive models to simulate the performance of multiferroic devices based upon this highly magnetostrictive material.

This research was supported at UCLA by the NSF Nanosystems Engineering Research Center for Translational Applications of Nanoscale Multiferroic Systems (TANMS) Cooperative Agreement (Award No. EEC-1160504) and FAME, one of six centers of STARnet, a Semiconductor Research Corporation program sponsored by MARCO and DARPA. Additionally, we acknowledge the support of the California Nano-Systems Institute for the utilization of their Molecular Instrumentation Center and Electron Imaging Center for NanoMachines.

[1] T. Wu, A. Bur, K. Wong, P. Zhao, C. S. Lynch, P. K. Amiri, K. L. Wang, and G. P. Carman, Appl. Phys. Lett. **98**, 478 (2011).
[2] M. Bibes and A. Barthelemy, Nat. Mater. **7**, 425 (2008).
[3] Y.-H. Chu, L. W. Martin, M. B. Holcomb, M. Gajek, S.-J. Han, Q. He, N. Balke, C.-H. Yang, D. Lee, W. Hu *et al.*, Nat. Mater. **7**, 478 (2008).

[4] A. K. Zvezdin, A. S. Logginov, G. A. Meshkov, and A. P. Pyatakov, Bull. Russ. Acad. Sci. **71**, 1561 (2007).

[5] M. Vopsaroiu, M. Cain, G. Sreenivasulu, G. Srinivasan, and A. Balbashov, Mater. Lett. **66**, 282 (2012).

[6] T. Nan, Y. Hui, M. Rinaldi, and N. X. Sun, Sci. Rep. **3**, 1985 (2013).

[7] M. Fiebig, J. Phys. D **38**, R123 (2005).

[8] P. Smole, W. Ruile, C. Korden, A. Ludwig, E. Quandt, S. Krassnitzer, and P. Pongratz, in *Frequency Control Symposium and PDA Exhibition Jointly with the 17th European Frequency and Time Forum, 2003*, Proceedings of the 2003 IEEE International Symposium (IEEE, Piscataway, NJ, 2003), pp. 903–906.

[9] J. Ma, J. Hu, Z. Li, and C.-W. Nan, Adv. Mater. **23**, 1062 (2011).

[10] H. Ba, M. Gajek, M. Bibes, and A. Barthlmy, J. Phys. Condens. Matter **20**, 434221 (2008).

[11] T. H. E. Lahtinen, K. J. A. Franke, and S. van Dijken, Sci. Rep. **2**, 258 (2012).

[12] N. Lei, T. Devolder, G. Agnus, P. Aubert, L. Daniel, J.-V. Kim, W. Zhao, T. Trypiniotis, R. P. Cowburn, C. Chappert *et al.*, Nat. Commun. **4**, 1378 (2013).

[13] P. Asselin and A. Thiele, IEEE Trans. Magn. **22**, 1876 (1986).

[14] R. H. Koch, J. G. Deak, D. W. Abraham, P. L. Trouilloud, R. A. Altman, Y. Lu, W. J. Gallagher, R. E. Scheuerlein, K. P. Roche, and S. S. P. Parkin, Phys. Rev. Lett. **81**, 4512 (1998).

[15] J. Gadbois, J. Zhu, W. Vavra, and A. Hurst, IEEE Trans. Magn. **34**, 1066 (1998).

[16] B. Zhu, C. C. H. Lo, S. J. Lee, and D. C. Jiles, J. Appl. Phys. **89**, 7009 (2001).

[17] Y. Shu, M. Lin, and K. Wu, Mech. Mater. **36**, 975 (2004).

[18] L. Banas, in *Numerical Analysis and Its Applications*, edited by Z. Li, L. Vulkov, and J. Waniewski, Lecture Notes in Computer Science Vol. 3401 (Springer, Berlin, 2005) pp. 158.

[19] C.-Y. Liang, S. M. Keller, A. E. Sepulveda, W.-Y. Sun, J. Cui, C. S. Lynch, and G. P. Carman, J. Appl. Phys. **116**, 123909 (2014).

[20] C.-Y. Liang, S. M. Keller, A. E. Sepulveda, A. Bur, W.-Y. Sun, K. Wetzlar, and G. P. Carman, Nanotechnology **25**, 435701 (2014).

[21] C.-Y. Liang, A. E. Sepulveda, D. Hoff, S. M. Keller, and G. P. Carman, J. Appl. Phys. **118**, 174101 (2015).

[22] J. Cui, C.-Y. Liang, E. A. Paisley, A. Sepulveda, J. F. Ihlefeld, G. P. Carman, and C. S. Lynch, Appl. Phys. Lett. **107**, 092903 (2015).

[23] K. Martens, D. L. Stein, and A. D. Kent, Phys. Rev. B **73**, 054413 (2006).

[24] G. D. ChavesOFlynn, K. Xiao, D. L. Stein, and A. D. Kent, J. Appl. Phys. **103**, 07D917 (2008).

[25] J. Z. Sun, R. P. Robertazzi, J. Nowak, P. L. Trouilloud, G. Hu, D. W. Abraham, M. C. Gaidis, S. L. Brown, E. J. O'Sullivan, W. J. Gallagher *et al.*, Phys. Rev. B **84**, 064413 (2011).

[26] J. X. Zhang and L. Q. Chen, Acta Mater. **53**, 2845 (2005).

[27] Y. Y. Huang and Y. M. Jin, Appl. Phys. Lett. **93**, 142504 (2008).

[28] K. Roy, S. Bandyopadhyay, and J. Atulasimha, J. Appl. Phys. **112**, 023914 (2012).

[29] A. K. Biswas, S. Bandyopadhyay, and J. Atulasimha, Appl. Phys. Lett. **103**, 232401 (2013).

[30] G. Dewar, S. Pagel, and P. Sourivong, Int. J. Mod. Phys. B **15**, 3266 (2001).

[31] E. Quandt, B. Gerlach, and K. Seemann, J. Appl. Phys. **76**, 7000 (1994).

[32] A. Speliotis, O. Kalogirou, and D. Niarchos, J. Appl. Phys. **81**, 5696 (1997).

[33] L. Rebouta, P. Martins, S. Lanceros-Mendez, J. M. Barandiaran, J. Gutierrez, L. C. Alvez, and E. Alves, J. Nano Research **18-19**, 235 (2012).

[34] C. de la Fuente, J. I. Arnaudas, L. Benito, M. Ciria, A. del Moral, C. Dufour, and K. Dumesnil, J. Phys. Condens. Matter **16**, 2959 (2004).

[35] K. P. Mohanchandra, S. V. Prikhodko, K. P. Wetzlar, W. Y. Sun, P. Nordeen, and G. P. Carman, AIP Adv. **5**, 097119 (2015).

[36] T. D. Rossing, J. Appl. Phys. **34**, 1133 (1963).

[37] X. Liu, Y. Y. Zhou, and J. K. Furdyna, Phys. Rev. B **75**, 195220 (2007).

[38] M. A. W. Schoen, J. M. Shaw, H. T. Nembach, M. Weiler, and T. J. Silva, Phys. Rev. B **92**, 184417 (2015).

[39] S. Klingler, A. V. Chumak, T. Mewes, B. Khodadadi, C. Mewes, C. Dubs, O. Surzhenko, B. Hillebrands, and A. Conca, J. Phys. D **48**, 015001 (2015).

[40] C. Kittel, Phys. Rev. **73**, 155 (1948).

[41] F. Schatz, M. Hirscher, M. Schnell, G. Flik, and H. Kronmüller, J. Appl. Phys. **76**, 5380 (1994).

[42] G. Dewar, J. Appl. Phys. **81**, 5713 (1997).

[43] F. Schreiber and Z. Frait, Phys. Rev. B **54**, 6473 (1996).

[44] P. I. Williams, D. G. Lord, and P. J. Grundy, J. Appl. Phys. **75**, 5257 (1994).